Geant4-BASED COMPREHENSIVE STUDY OF THE ABSORBED FRACTION FOR ELECTRONS AND GAMMA-PHOTONS USING VARIOUS GEOMETRICAL MODELS AND BIOLOGICAL TISSUES

by

***Ziaur RAHMAN*[1], *Shakeel Ur REHMAN*[2], *Sikander M. MIRZA*[2], *Waheed ARSHED*[1], *and Nasir M. MIRZA*[2*]**

[1]Health Physics Division, Pakistan Institute of Nuclear Science & Technology, Nilore, Islamabad, Pakistan
[2]Department of Physics & Applied Mathematics, Pakistan Institute of Engineering & Applied Sciences, Nilore, Islamabad, Pakistan

Scientific paper
DOI: 10.2298/NTRP1304341R

The Geant4-based comprehensive model has been developed to predict absorbed fraction values for both electrons and gamma photons in spherical, ellipsoidal, and cylindrical geometries. Simulations have been carried out for water, ICRP soft-, brain-, lung-, and ICRU bone tissue for electrons in 0.1 MeV-4 MeV and γ-photons in the 0.02 MeV-2.75 MeV energy range. Consistent with experimental observations, the Geant4-simulated values of absorbed fractions show a decreasing trend with an increase in radiation energy. Compared with NIST XCOM and ICRU data, the Geant4-based simulated values of the absorbed fraction remain within a 4.2% and 1.6% deviation, respectively. For electrons and γ-photons, the relative difference between the Geant4-based comprehensive model predictions and those of Stabin and Konijnenberg's re-evaluation remains within a 6.8% and 7.4% range, respectively. Ellipsoidal and cylindrical models show 4.9% and 10.1% higher respective values of absorbed dose fractions relative to the spherical model. Target volume dependence of the absorbed fraction values has been found to follow a logical behavior for electrons and Belehradek's equation for γ-photons. Gamma-ray absorbed fraction values have been found to be sensitive to the material composition of targets, especially at low energies, while for elections, they remain insensitive to them.

Key words: Geant4 simulation, energy deposition, internal dosimetry, absorbed fraction

INTRODUCTION

Monte Carlo methods are commonly used to simulate radiation transport in many fields of sciences – such as nuclear engineering, radiotherapy, diagnostic radiology, radiation protection, and nuclear medicine – to estimate the radiation flux, energy deposition profiles and other physical quantities of interest [1]. With advancements in computer technology, treatment planning systems based on Monte Carlo simulations are now commercially available for medical purposes [2].

Direct measurement of the absorbed dose to various body organs, due to some diagnostic or therapeutic procedures, or due to exposure to accidental releases from nuclear installations, is very difficult. Standard methodologies used for absorbed dose estimation have been developed by the international commission on radiological protection (ICRP) and medical internal radiation dose (MIRD), a committee of the Society of Nuclear Medicine [3]. From a physics viewpoint, both methodologies are consistent with each other. Their dosimetric formalism is based on radionuclide characteristics, the distance of the target organ from source organs, biological parameters of the source organ, and energy absorption in the target organ emitted by the source organ. The ICRP dosimetric model is based on risk assessment of the biological effect of ionizing radiation [4].

The formalism of MIRD has long been adopted as the standard calculation method for the estimation of radiation doses to organs from radionuclides distributed in the body. The MIRD absorbed dose calculation consists of time integrated activity in the organ, multiplied by the corresponding *S*-value (mean absorbed dose to a target organ per nuclear transformation of the radionuclide in the source organ) [5]. The time integrated activity can be estimated by applying the biokinetic model of the source organ or by employing SPECT or PET quantitative imaging techniques.

* Corresponding author; e-mail: nmm@pieas.edu.pk

The *S*-values of an organ can be estimated by using a specific absorbed fraction (SAF) in that target structure/tissue for the corresponding radionuclide of interest. SAF values can be evaluated by estimating the energy deposition in the selected tissue/target. Absorbed fractions for uniformly distributed tissues can be evaluated by Monte Carlo codes [6, 7], Point Kernels or by analytical methods [8]. The SAF or AF (absorbed fraction) values in this study primarily rely on Monte Carlo radiation transport calculations using computational anatomical models, also known as virtual human phantoms.

Loevinger and Berman first introduced the concept of AF for absorbed dose estimation. Their work was published in the first issue of MIRD publications. Since then, the methodology developed by Loevinger has been accepted and used by a majority in the scientific community working in the area of nuclear medicine and radiation protection [5]. Later on, Berger evaluated energy absorption by implementing the moment analytical method for γ-photons from point sources in spheres of various sizes, using water as material. The energy deposition for monoenergetic γ-photons of an energy range of 0.015 MeV to 3 MeV was considered. The data was published in MIRD pamphlet No. 2, along with the build-up factors and other related data in a tabulated form [8]. Brownell *et al*. estimated the photon absorbed fraction for cylindrical, spherical and ellipsoidal volumes using Monte Carlo calculations, with the details presented in MIRD pamphlet No. 3. AF values were estimated in tissue-equivalent material for spheres and cylinders of masses ranging from 2 kg to 200 kg and ellipsoids of mass ranging from 0.3 kg to 6 kg, for photon energies in the 0.02 MeV-2.75 MeV range [9].

Akabani *et al*. evaluated the AF values in small tumors modeled by spheres sizing 10^{-3} to 2 10^{-2} m in radius. They used EGS as the Monte Carlo code for the evaluation of the absorbed fraction in small tissue equivalent material uniformly distributed spheres for beta radiations from a number of selected radionuclides. An energy range of 0.05 MeV to 4 MeV was considered for monoenergetic electrons, using cutoff energies of 10 and 1 keV for electrons and γ-photons, respectively, as simulation parameters [10].

The absorbed fraction values were estimated by Siegel and Stabin for spherical, uniformly distributed β^- and electron sources of various sizes (of masses up to 1000 g), within the energy ranges of 0.062 MeV to 1.428 MeV and 0.025 MeV to 4 MeV, respectively, using Berger's analytical methodology [11]. Their study reevaluated absorbed fraction values for γ-photons and electrons in homogeneous spheres of the unit density tissue-equivalent composition of various sizes. AF values for electrons and γ-photons were published in MIRD pamphlets 3 and 8, powered by two modern Monte Carlo codes: EGS4 and MCNP-4B. The energy ranges for electrons and γ-photons of 0.1 MeV to 4 MeV and 0.02 MeV to 2.75 MeV were considered, respectively. The authors recommend an average value of the two Monte Carlo codes for AF, for all spherical sizes and energies, for both electrons and γ-photons [11].

The absorbed fractions were estimated by Amato *et al*. for ellipsoidal, uniformly distributed γ-photons and monoenergetic electrons of various sizes in the energy range of 0.01 MeV to 1 MeV and 0.01 MeV to 2 MeV, respectively, using the Geant4 Monte Carlo code [12]. ICRP (Publication 89) soft tissue was adopted as the material for said modeled volumes [13, 14]. Helio *et al*. also presented the absorbed fraction data for electron and γ-photons in uniformly distributed spheres of various sizes, using the MCNP and Geant4 Monte Carlo codes. Water, ICRU44 soft tissue, red bone marrow, bone, and lung tissues, were adopted as constituent materials for all spherical volumes [15].

To the best of our knowledge, there are no published data of absorbed fractions for uniformly distributed cylindrically modeled targets. The existing work is limited to water and ICRU soft tissue only while, in practice, a wide variety of other types of tissue are encountered, including brain, lung and bone tissue. Also, current studies are confined to a limited range of sizes as well as energy values. In practice, one may encounter much larger ranges in both cases. To our understanding, a comprehensive model that covers all three geometries – the ellipsoidal, spherical and cylindrical ones – does not exist for both electrons and photons.

The goal of this paper is to evaluate the discrepancies in the estimation of the absorbed fractions for photon and electron sources in various geometrical models in relation to different biological tissues as material, using the Geant4 Monte Carlo code which, nowadays, is among the most worldwide used code, employed by medical physicists for dose estimation originating from external, as well as from internal radiation sources [16]. In this study, we have employed spherical, ellipsoidal, and cylindrical geometrical models. The spherical model is employed to represent nodules and tumors or other small uptake regains. Ellipsoidal models are used to model not only small target tissue such as thyroid nodules, but also entire organs like kidneys, ovaries, spleen, tactical, thymus, and bladder. The human trunk, small and large intestine, head, neck, and extremities are modeled cylindrically.

The absorbed fractions for electrons and photons distributed uniformly in spheres and ellipsoids have been reported by many authors. In this work, the study was extended to cylindrical geometry and an overall picture of the absorbed fraction for the three geometrical models of various sizes and a range of photon and electron energies. Further simulations have been carried out for water, ICRP soft, brain, lung, and ICRU bone tissue as the material for these models.

The energy range adopted in our study covers most of the energies emitted by radionuclides currently employed in nuclear medicine procedures or any accidental inhalation/injection of radionuclides. The energy range considered for electrons is 0.1 MeV to 4 MeV, while that for γ-photons is 0.02 MeV to 2.75 MeV.

For the validation of our code, we have compared the Geant4-based AF for γ-photons and electrons with the already published AF data. The Geant4-based total cross-section for γ-photons and CSDA (continuous slowing down approximation) range of electrons were intercompared with the NIST XCOM cross-section data and ICRU report 37, respectively [17, 18].

MATERIAL AND METHODS

In nuclear medicine, several procedures are in use as diagnostic and therapeutic tools. Radiopharmaceuticals are administered to patients orally or intravenously. When a radionuclide enters the organ, it acts as a source which irradiates the rest of the organs as well as the body itself, up to its physical decay or excretion from the body. The magnitude of the absorbed dose to various organs depends on the characteristics of the radionuclide, distance of the target organ from source organs and the absorbed fraction (AF) or specific absorbed fraction $\Phi(T \quad S)$ defined as

$$\Phi(T \quad S) \quad \frac{\phi(T \quad S)}{m_{\mathrm{T}}} \tag{1}$$

where $\phi(T \quad S)$ is the absorbed fraction and m_{T} – the mass of the target. The absorbed fraction is defined as

$$\phi(T \quad S) \quad \frac{E_{\mathrm{T}}}{E_{\mathrm{S}}} \tag{2}$$

where E_{T} is the deposited energy in the target of interest and E_{S} – the energy emitted by the source region. In this simulation, both the target and the source are the same.

Geant4 is a Monte Carlo simulation tool kit for radiation transport. For the simulations, Geant4 utilizes the full functionality of hadronic, electromagnetic and optical physics [12]. Geant4 offers PENELOPE, LIVERMORE, and STANDARD physics models for low and high-energy particle simulations. Worldwide, the scientific community uses Geant4 in accelerator physics, particle physics, astrophysics, medical physics and high energy physics (HEP) experiments, due to its flexibilities in physics models and processes. The validity and accuracy of Geant4 physics models and processes for electrons and γ-rays has been studied by several authors, with the corresponding discrepancies presented [19].

In our simulations, the Geant4 standard electromagnetic physics model has been employed for all physics processes. The package covers energies ranging from 1 keV to 100 TeV for electron and γ-ray transportation. Physics processes such as Compton scattering, electron-positron pair production and the photoelectric effect were taken into account for γ-ray transportation. Bremsstrahlung and Moller scattering for electron and Bhabha scattering for positron are also available physics processes in this model.

In order to check the physics processes of the Geant4 electromagnetic Standard Physics model, we have compared the total cross-section for γ-photons and CSDA range of electrons with the published data. For this purpose, the Geant4-based total cross-section for γ-photons and CSDA range of electrons were intercompared with the NIST XCOM cross-section data and ICRU report 37, respectively [17, 18].

Absorbed fractions for electrons and photons distributed uniformly in spheres, cylinders and ellipsoids have been estimated. The absorbed fraction for each value of the particle energy is estimated by the energy deposition in the target. Principle axes 1/1/0.75 and 1/0.50 for the cylinder and the ellipsoid, respectively, were considered in this work. Further simulations for water, ICRP soft, brain, lung & ICRU bone tissue as material for these models were carried out. The elemental composition of the material used in our simulations is shown in tab. 1. The energy range adopted in this study covers most of the energies emitted by radionuclides currently used in nuclear medicine procedures or any accidental inhalation/ingestion of radionuclides. For electrons, the energy range of 0.1 MeV to 4 MeV and, for γ-photons, that of 0.02 MeV to 2.75 MeV, were considered. Stabin's and Konijnenberg's suggested ranges of volume for spherical and ellipsoidal shapes were also considered, for both γ-photons and electrons [11]. In cylindrical geometry, volume values up to 0.1 m^3 were considered in order to meet the requirements of the fraction absorbed by the human trunk.

For good statistical results, 10^7 histories (number of particles) were generated for each calculation point in Geant4 simulations. The relative difference between the reference value and the Geant4 calculated value is found as Δ_{Geant4} calculated by

$$\Delta_{\mathrm{Geant4}} \quad \frac{\phi_{\mathrm{Geant\,4}} \quad \phi_{\mathrm{ref}}}{\phi_{\mathrm{ref}}} \quad 100 \tag{3}$$

where Δ_{Geant4} is the Geant4-based absorbed fraction, while ϕ_{ref} corresponds to the value of the absorbed fraction of reference. Statistical uncertainties estimated in the simulated results are below 1%. All simulations conducted in this work were carried out using the Geant4 version 9.5.

RESULTS AND DISCUSSION

Comparison of microscopic and macroscopic quantities

Geant4 simulations are validated by the comparison of simulation results with published data. For this

Table 1. Elemental composition of ICRP soft, brain, lung, and ICRU bone tissue material, as given in Geant4 material definitions

Item	ICRP-soft tissue	ICRP-lung	ICRP-brain	ICRP-bone	Water
Density [gcm^{-3}]	1.04	1.05	1.03	1.85	1
Excitation energy [eV]	72.3	75.3	73.3	91.9	75
Composition					
H	0.104472	0.101278	0.110667	0.063984	0.112
C	0.23219	0.10231	0.12542	0.278	
N	0.02488	0.02865	0.01328	0.027	
O	0.630238	0.757072	0.737723	0.410016	0.888
Na	0.00113	0.00184	0.00184		
Mg	0.00013	0.00073	0.00015	0.002	
P	0.00133	0.0008	0.00354	0.07	
S	0.00199	0.00225	0.00177	0.002	
Cl	0.00134	0.00266	0.00236		
K	0.00199	0.00194	0.0031		
Ca	0.00023	9E-05	9E-05	0.147	
Fe	5E-05	0.00037	5E-05		
Zn	3E-05	1E-0	1E-05		

purpose, two types of validation are performed. First the microscopic quantities such as the total cross-section of gamma photons and CSDA range of electrons in water were compared. Then macroscopic quantities, including simulation outcomes such as the energy deposited in unit density tissue spheres, were compared with the published data. Microscopic quantities, including the total cross-section of γ-photons and CSDA range of electrons, are compared with NIST XCOM data, ICRU report 37, respectively, for water. Figure 1. shows the variation of the total cross-section of γ-photons used in Geant4 simulations, along with the percentage error, for the energy range of 10 keV to 100 MeV. The relative difference of Geant4 and NIST XCOM data remains within 4.2%. Similarly, the CSDA range of electrons was compared with ICRU report 37 data for water. Figure 2 shows the comparison of the two data sets for a range of energies. The

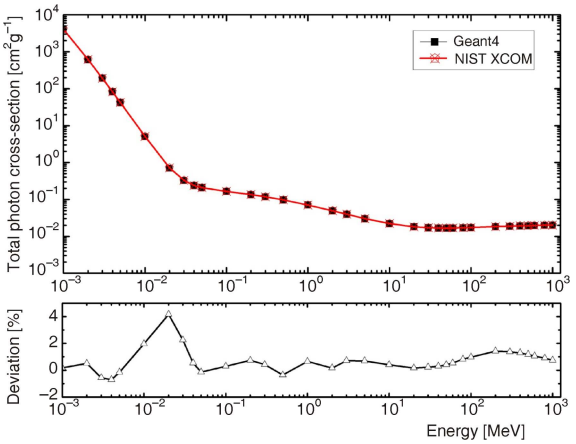

Figure 1. Total cross-sections of photon interactions in water for the Geant4 standard electromagnetic physics model and NIST XCOM, and percentage difference b/w the results of Geant4 and NIST XCOM data

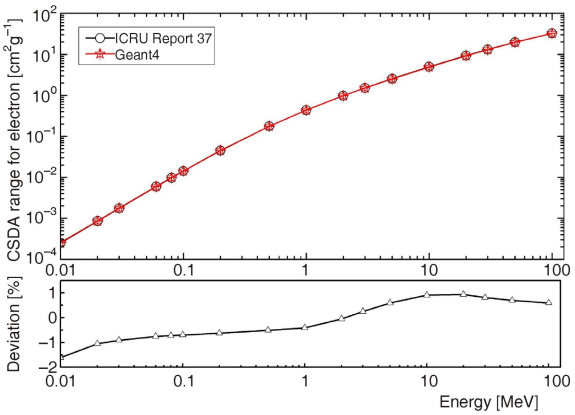

Figure 2. Variation of CSDA ranges for electrons with energy in water using the Geant4 standard electromagnetic model and ICRU 37 report, and percentage differences in CSDA ranges of electron b/w Geant4 and ICRU 37 results

percentage differences between the two data sets shown in fig. 2 amounted up to 1.6%.

For the validation of Geant4 simulations, we have compared the absorbed fraction results with Stabin and Konijnenberg data, estimated for spherically uniform distributed electron sources of various sizes (masses 0.01 g to 1000 g range) in the energy ranges of 0.02 MeV to 4 MeV, respectively. Table 2 shows the comparison of the two data. It presents the Geant4-computed absorbed fraction values, along with parentage deviations from Stabin and Konijnenberg data for a range of energies and sizes. The relative differences between the two data sets range from 0.09% to 6.8% over the entire energy and size range considered in this work. Similarly, tab. 3 presents Geant4-computed absorbed fraction values for γ-photons, along with the parentage deviation from Stabin and Konijnenberg data for a range of energies

Table 2. Absorbed fractions for electrons (Geant4 simulation) in spheres of various sizes [g] and energies [MeV]; comparison of Geant4 results with the % difference (in brackets) to Stabin and Konijnenberg results

Mass [g]	E_e [MeV]						
	0.1	0.2	0.4	0.7	1	2	4
0.01	0.958 (–0.5)	0.868 (0.5)	0.643 (–0.2)	0.346 (2.2)	0.205 (4.5)	0.090 (4.8)	0.043 (3.3)
1	0.991 (–0.1)	0.972 (0.1)	0.921 (0.0)	0.839 (0.8)	0.755 (1.8)	0.505 (6.8)	0.227 (6.8)
10	0.996 (0.0)	0.986 (–0.1)	0.962 (0.1)	0.925 (0.5)	0.884 (0.8)	0.750 (1.9)	0.506 (4.4)
20	0.996 (–0.1)	0.989 (0.0)	0.971 (0.2)	0.939 (0.4)	0.907 (0.6)	0.800 (1.5)	0.592 (3.0)
40	0.997 (0.0)	0.991 (0.0)	0.977 (0.2)	0.953 (0.4)	0.925 (0.5)	0.839 (1.6)	0.666 (2.0)
60	0.997 (0.0)	0.992 (0.0)	0.980 (0.2)	0.957 (0.1)	0.935 (0.4)	0.857 (1.2)	0.705 (2.1)
100	0.998 (0.0)	0.993 (0.0)	0.982 (0.0)	0.964 (0.2)	0.945 (0.5)	0.879 (0.9)	0.748 (1.5)
500	0.999 (0.1)	0.996 (0.0)	0.989 (0.1)	0.978 (0.2)	0.967 (0.3)	0.928 (0.5)	0.846 (0.9)
1000	0.999 (0.0)	0.997 (0.1)	0.991 (0.0)	0.982 (0.2)	0.973 (0.2)	0.941 (0.4)	0.875 (0.7)

Table 3. Absorbed fractions for photons in spheres of various sizes [g] and energies [MeV]; comparison of Geant4 results with the % difference (in brackets) to Stabin and Konijnenberg results

Mass [g]	E_γ [MeV]						
	0.080	0.100	0.140	0.364	0.662	1.460	2.750
2	0.016 (2.57)	0.016 (7.36)	0.016 (3.08)	0.019 (–1.41)	0.018 (–0.09)	0.013 (5.09)	0.007 (–2.34)
4	0.021 (5.64)	0.021 (2.56)	0.021 (0.33)	0.024 (2.82)	0.023 (3.89)	0.017 (–1.20)	0.010 (–2.00)
6	0.024 (6.47)	0.023 (2.15)	0.024 (0.86)	0.027 (1.68)	0.026 (1.34)	0.020 (1.98)	0.012 (0.31)
8	0.027 (4.79)	0.026 (4.50)	0.027 (2.65)	0.030 (4.60)	0.030 (6.73)	0.023 (5.34)	0.014 (–1.21)
10	0.030 (5.38)	0.028 (4.75)	0.029 (3.14)	0.033 (2.46)	0.032 (3.93)	0.025 (3.38)	0.015 (–3.33)
20	0.038 (3.67)	0.036 (4.00)	0.037 (2.91)	0.041 (3.14)	0.041 (3.88)	0.032 (3.24)	0.022 (2.42)
40	0.050 (5.96)	0.047 (4.16)	0.047 (3.11)	0.052 (2.04)	0.051 (4.52)	0.042 (3.88)	0.029 (3.76)
60	0.058 (6.32)	0.055 (5.78)	0.055 (3.62)	0.060 (3.49)	0.059 (5.72)	0.047 (2.37)	0.034 (–0.98)
100	0.072 (6.82)	0.067 (5.38)	0.066 (4.43)	0.071 (3.17)	0.069 (2.82)	0.057 (2.89)	0.041 (–0.07)
500	0.134 (1.89)	0.124 (2.79)	0.119 (0.70)	0.122 (1.16)	0.118 (2.86)	0.096 (0.33)	0.074 (–2.10)
1000	0.176 (2.45)	0.162 (2.54)	0.153 (1.61)	0.153 (1.39)	0.148 (2.67)	0.123 (2.62)	0.095 (–0.92)

and sizes. A maximum difference of 7.36% in corresponding values between the two data sets was found in a few cases. It is clear from tab. 3 that, at low energies, the difference is relatively more prominent for high values of energies.

The observed discrepancy may be due to differences in the basic physics data sets used by Stabin and those used by the Geant4 program. Other minor variances can possibly be due to the differences in the material used in the two simulations. Water and tissue-equivalent materials used by Stabin and Konijnenberg have the same atomic densities, but different atomic compositions. It has been shown by Ellett and Humes that, for photon energies less than 100 keV, the absorbed fraction is increasingly sensitive to atomic composition. In these simulations, the observed differences are more prominent at low energies than at high ones. For electrons, no significant difference was found over the entire energy range employed here.

Absorbed fraction for gamma photons and electrons

Absorbed fraction values for γ-photons and electrons for various energies, geometrical models and tissue composition are shown in figs. 3, 4, and 5 for γ-rays and in tabs. 4, 5, and 6 for electrons. The absorbed fraction for electrons has a much higher value than that of γ-photons of the same volume and energy. The reason for this is the direct Columbic interaction of electrons with atomic nuclei and electrons. Bremsstrahlung radiation leakage reduces the absorbed fraction value slightly, depending on the energy of the electrons. Penetrating γ-radiation interacts indirectly, thereby increasing the chance of escape from the target, resulting in the small value of the absorbed fraction.

We generalize the relation between the absorbed fraction for the electron and target volume V, which gives us the following logistic equation fit. Further on, fitting parameters for spherical, ellipsoidal and cylindrical models were analyzed. Fitting parameters for all models are shown in tab. 7. Parameters A_1 and A_2 represent the range of values of fit, respectively, depending on the corresponding volume range. Parameter V_o is the mid-value of fit. The most sensitive value is exponent P of the fit function which defines how quickly the absorbed fraction increases as the volume for a given energy increases. Fitted P values 0.39, 0.33, and 0.32 were obtained for spherical, ellipsoidal, and cylindrical models, respectively. The four parameters shown here depend on the energy of the electron

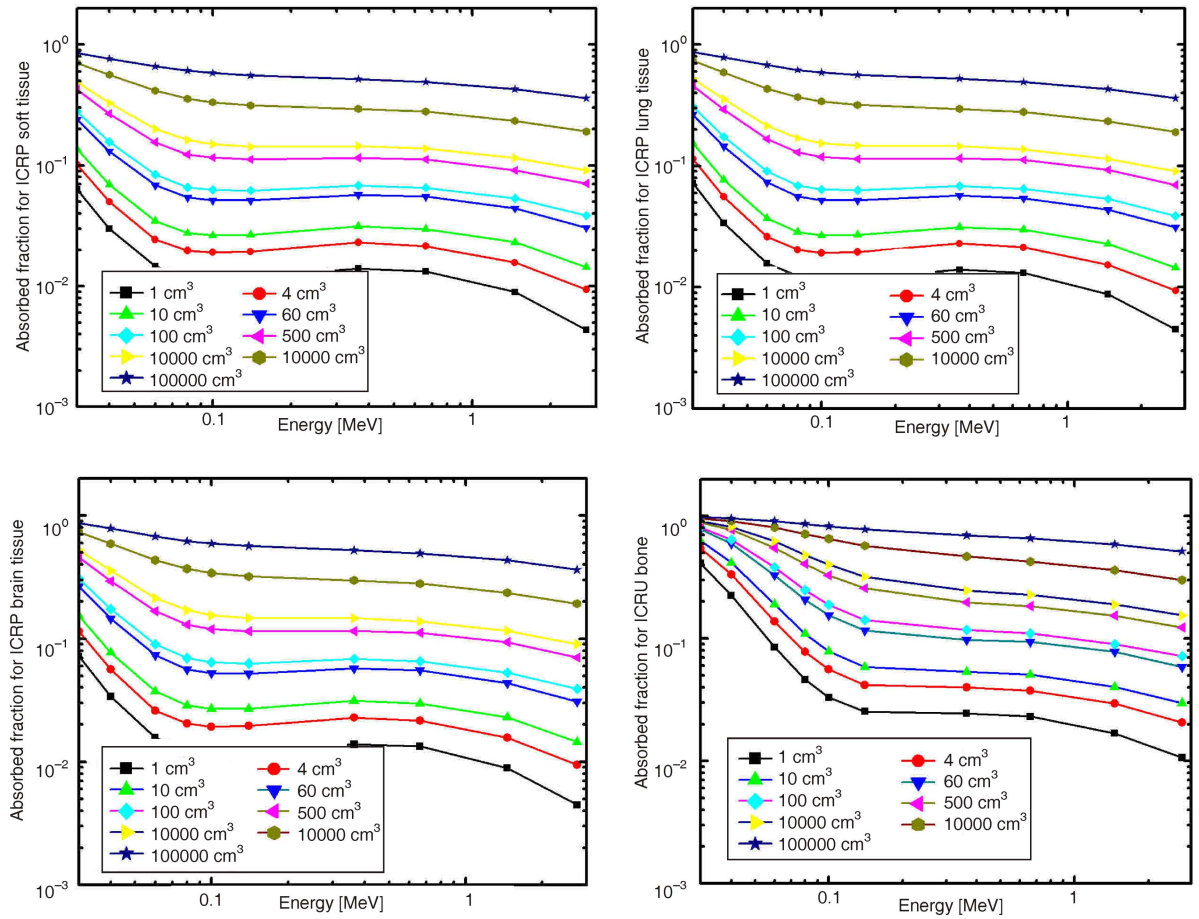

Figure 3. Absorbed fraction in cylindrical targets for various photon energies, using ICRP soft tissue, ICRP lung tissue, ICRP brain tissue, and ICRU bone as a material

$$\phi \quad (A_1 \quad A_2)\,1 \quad \frac{V}{V_o}^{P \quad 1} \qquad A_2 \qquad (4)$$

A similar generalization has also been carried out for the γ-photon absorbed fraction and target volume V, resulting in the following Belehradek equation fit [20]. The fitting parameters were, further, analyzed for spherical, ellipsoidal, and cylindrical models. Fitting parameters for all models and R^2-values which show a good fit are shown in tab. 8 (where α is the coefficient of the power function, b – the position parameter, and C – the slope of $\log\phi$ and $\log V$ plot). The position parameter varies, depending on the range of the volume selected for the models. Parameter C is the power of the fit, showing a high value for the spherical model, in comparison to the other two models

$$\phi \quad a(V \quad b)^c \qquad (5)$$

Variation of the absorbed fraction with volume for identical geometrical models

Absorbed fraction variation values for various sizes of cylindrical, elliptical, and spherical models are shown in figs. 3, 4, and 5, respectively, for a range of photon energies and tissues. It can be seen that the absorbed fraction at low energies has higher values because of the large photoelectric absorption cross-section values. Consequently, in the low energy range, more energy is deposited, even in cases of small size shapes. The absorbed fraction is not sensitive within the energy range of 0.1 MeV to 1 MeV. Although there is a slight variation in the absorbed fraction as the energy increases within the range, this may be due to an increase in the Compton scattering probability. However, in this energy range, the increased transmission of high-energy γ-photons is largely compensated by the increase in the energy transfer from first collision Compton events, this being more prominent in relation to small volumes.

For targets with small volumes, the large value of surface-to-volume ratio entails higher leakage, thereby reducing the value of the absorbed fraction. For large targets, the increase in the absorbed fraction is due to multiple Compton events and lesser transmission of high energy γ-photons and electrons due to the small surface-to-volume ratio. The increase in the absorbed fraction pattern regarding energy is identical for all geometrical models.

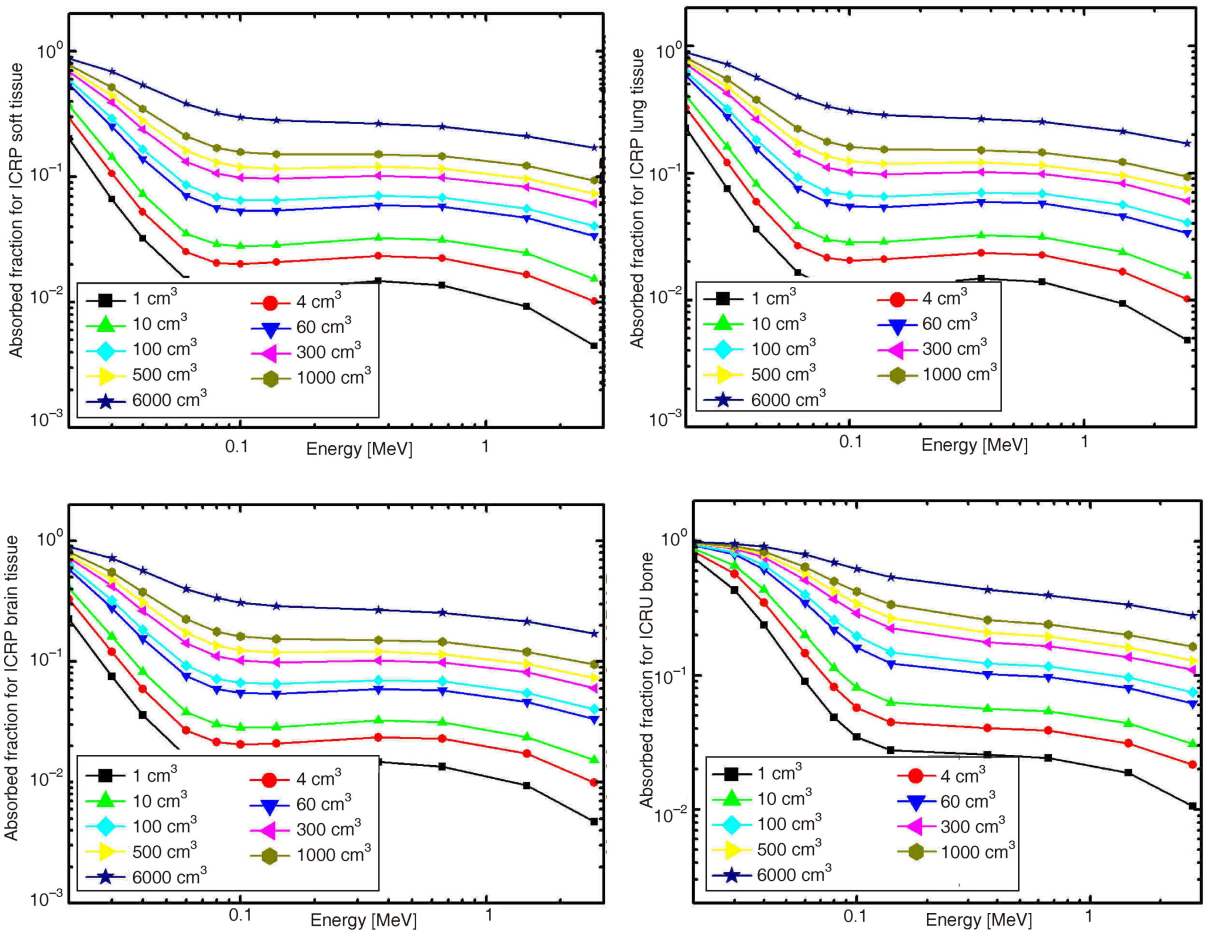

Figure 4. Absorbed fraction in ellipsoidal targets for various photon energies, using ICRP soft tissue, ICRP lung tissue, ICRP brain tissue, and ICRU bone as a material

Absorbed fraction for various geometrical models of the same size

The variation of absorbed fraction values for three different geometrical models, 6 10^{-3} m^3 in size, is shown in fig. 6. For the sphere, absorbed fraction values are 4.9% and 10.1% higher than those of ellipsoidal and cylindrical models, respectively, over the entire energy range. The relative difference among the absorbed fraction results of ellipsoidal and cylindrical models is 5.8%. Absorbed fraction values increase with volume, because of the increasing volume-to-surface ratio for each type of model. The increase in volume causes the fraction of radiations escaping from the target to decrease, thereby increasing the absorbed energy of radiations. However, the slight difference in the absorbed fraction of the cylindrical model is due to the small value of the volume-to-surface ratio, resulting in higher escape rates from the cylindrical model, as compared to elliptical and spherical models [21].

Absorbed fraction for different tissue compositions and materials

Tables 4-6 for electrons and figs. 3-5 for γ-photons present the absorbed fraction values for different tissue compositions. For the electron, absorbed fraction values are nearly independent from the tissue composition of the material, but do depend on the atomic density of the material. Absorbed fraction values for ICRU bone tissue are higher, as expected, due to the corresponding higher values of atomic density. A maximum relative difference in absorbed fraction values between ICRU bone and ICRP brain tissue is 17% for low energies and 46% for high energies, respectively, for all target sizes and shapes. Absorbed fraction values for electrons are nearly independent of the geometrical models of the same tissue composition. The difference in absorbed fraction values for ICRP soft tissue and water is below 1% for low energy and 4% for high energy, respectively. The composition of soft tissue and water is different, but the absorbed fraction values are not sensitive to material composition at low energy levels.

For γ-photons, the absorbed fraction is dependent on material composition, even for materials of the same density. A high value of density of the material results in higher photon interaction probability, leading to a high value of the absorbed fraction. Atomic densities of ICRP lung, brain and soft tissues are nearly the same. Consequently, no appreciable differences in absorbed fraction values were found over the entire range of energies and sizes. However, there is

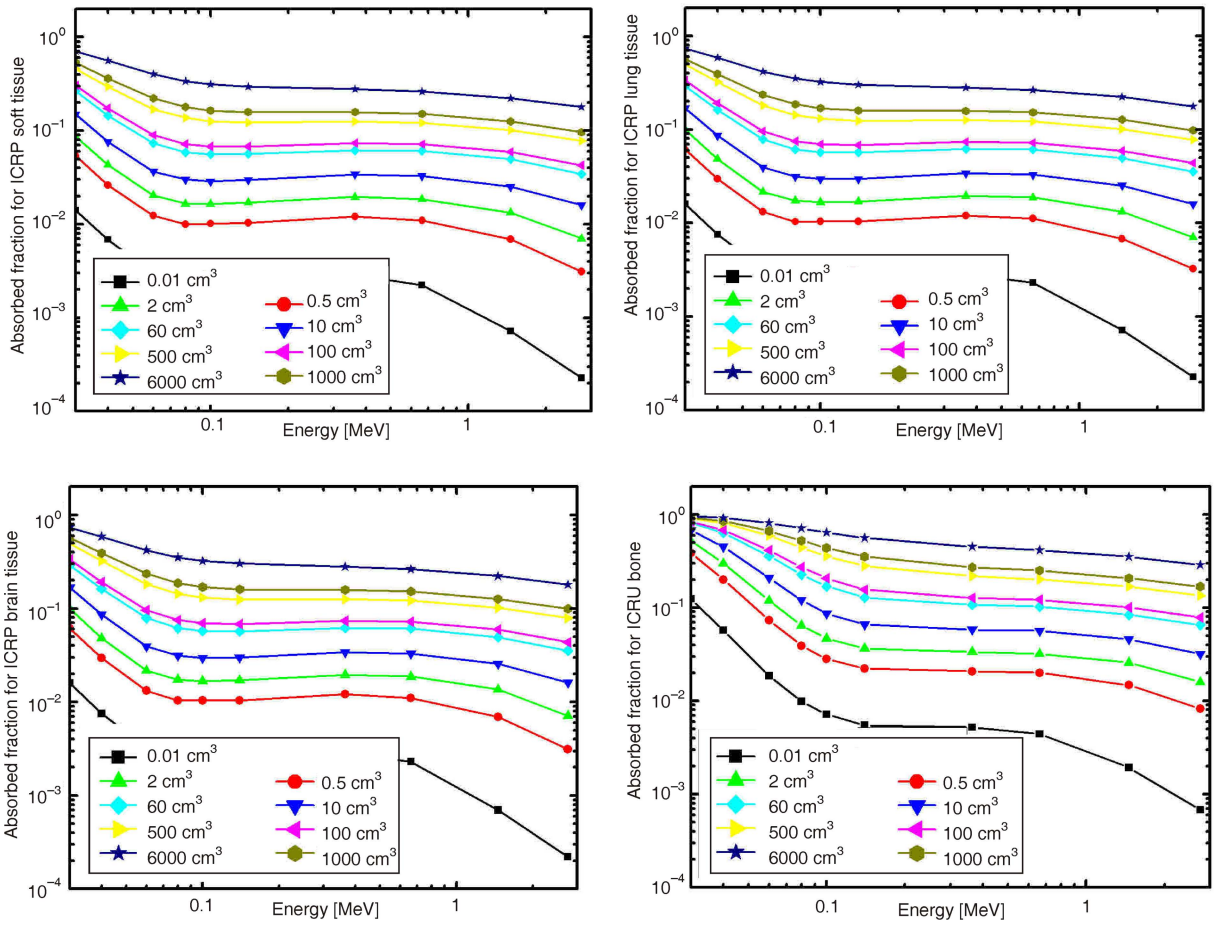

Figure 5. Absorbed fraction in spherical targets for various photon energies, using ICRP soft tissue, ICRP lung tissue, ICRP brain tissue, and ICRU bone as a material

Table 4. Variation of absorbed fraction values with the target volume in cylindrical targets for various electron energies, using water (W), ICRP soft tissue (ST), ICRP lung tissue (LT), ICRP brain tissue (BT), and ICRU bone (BO) as material

Volume [cm^3]	Absorbed fraction value																			
	0.1 MeV					1 MeV					2 MeV					4 MeV				
	W	ST	LT	BT	BO	W	ST	LT	BT	BO	W	ST	LT	BT	BO	W	ST	LT	BT	BO
1	0.989	0.989	0.989	0.989	0.994	0.706	0.719	0.714	0.716	0.823	0.451	0.462	0.462	0.461	0.635	0.209	0.218	0.216	0.213	0.379
4	0.993	0.993	0.993	0.993	0.996	0.810	0.816	0.814	0.816	0.886	0.617	0.628	0.630	0.629	0.759	0.343	0.356	0.354	0.354	0.551
10	0.994	0.995	0.995	0.995	0.997	0.856	0.861	0.860	0.862	0.913	0.706	0.717	0.715	0.717	0.817	0.449	0.466	0.464	0.464	0.649
20	0.996	0.996	0.996	0.996	0.998	0.885	0.889	0.889	0.889	0.931	0.760	0.768	0.786	0.769	0.853	0.536	0.550	0.546	0.549	0.712
40	0.996	0.997	0.997	0.997	0.998	0.906	0.910	0.910	0.909	0.944	0.806	0.810	0.811	0.810	0.881	0.612	0.626	0.623	0.625	0.762
100	0.997	0.998	0.998	0.998	0.999	0.931	0.933	0.933	0.933	0.958	0.853	0.860	0.858	0.858	0.910	0.704	0.712	0.709	0.711	0.818
500	0.998	0.998	0.998	0.998	0.999	0.958	0.960	0.959	0.960	0.975	0.909	0.914	0.913	0.913	0.946	0.813	0.821	0.819	0.818	0.887
1000	0.999	0.999	0.999	0.999	0.999	0.966	0.967	0.966	0.967	0.979	0.982	0.929	0.929	0.930	0.955	0.849	0.852	0.853	0.852	0.906
10000	0.999	0.999	0.999	0.999	1.000	0.983	0.984	0.984	0.983	0.990	0.963	0.965	0.965	0.965	0.977	0.923	0.922	0.926	0.926	0.953
50000	1.000	1.000	1.000	1.000	1.000	0.990	0.990	0.990	0.990	0.994	0.977	0.979	0.979	0.978	0.987	0.953	0.955	0.954	0.954	0.971
100000	1.000	1.000	1.000	1.000	1.000	0.991	0.992	0.992	0.992	0.995	0.982	0.983	0.983	0.983	0.989	0.962	0.963	0.962	0.963	0.977

some difference pertaining to the results of water with ICRP lung tissue, found to be 9% below 100 keV and 5% above 100 keV. The relative difference in the absorbed fraction of ICRU bone tissue in comparison to all other tissues is 85%. This may be attributed to the higher values of the atomic number and the density of the bone material.

Absorbed fraction values computed using various low-energy physics models available in Geant4 have been compared with those of the standard physics model for different secondary cut values. Table 9 shows a good agreement between the three models regarding the deposition of 20 keV photons. From the Table, it is clear that the standard model predicts an energy deposition which is up to 6.04% and 6.49% less than the Livermore and Penelope models, respectively, for all sphere sizes and range cut values considered in this study. This behavior can be explained by the differences in the total photon cross-sections employed in said Geant4 models. These observations are

Table 5. Variation of absorbed fraction values with the target volume in ellipsoidal targets for various electron energies, using water (W), ICRP soft tissue (ST), ICRP lung tissue (LT), ICRP brain tissue (BT), and ICRU bone (BO) as material

Volume [cm^3]	Absorbed fraction value																			
	0.1 MeV					1 MeV					2 MeV					4 MeV				
	W	ST	LT	BT	BO	W	ST	LT	BT	BO	W	ST	LT	BT	BO	W	ST	LT	BT	BO
1	0.990	0.991	0.991	0.990	0.995	0.737	0.746	0.745	0.745	0.845	0.483	0.498	0.495	0.493	0.670	0.219	0.230	0.228	0.229	0.409
4	0.993	0.994	0.994	0.994	0.996	0.831	0.839	0.837	0.837	0.899	0.648	0.663	0.658	0.657	0.786	0.361	0.375	0.375	0.374	0.582
10	0.995	0.996	0.995	0.995	0.997	0.875	0.879	0.877	0.878	0.926	0.734	0.742	0.744	0.743	0.840	0.482	0.494	0.491	0.492	0.677
20	0.996	0.996	0.996	0.996	0.998	0.899	0.904	0.903	0.902	0.490	0.786	0.792	0.792	0.793	0.871	0.567	0.581	0.580	0.580	0.738
40	0.997	0.997	0.997	0.997	0.998	0.918	0.923	0.922	0.923	0.952	0.828	0.834	0.832	0.834	0.895	0.643	0.656	0.658	0.656	0.787
100	0.998	0.998	0.998	0.998	0.999	0.940	0.943	0.943	0.943	0.964	0.871	0.875	0.875	0.874	0.921	0.732	0.740	0.737	0.740	0.839
500	0.998	0.999	0.999	0.999	0.999	0.964	0.966	0.965	0.966	0.978	0.921	0.925	0.925	0.924	0.950	0.835	0.841	0.840	0.839	0.900
1000	0.999	0.999	0.999	0.999	0.999	0.971	0.973	0.972	0.971	0.982	0.937	0.939	0.939	0938	0.961	0.866	0.872	0.869	0.871	0.918
6000	0.999	0.999	0.999	0.999	1.000	0.983	0.984	0.984	0.984	0.990	0.963	0.965	0.965	0.964	0.977	0.922	0.926	0.923	0.924	0.951

Table 6. Variation of absorbed fraction values with the target volume in spherical targets for various electron energies, using water (W), ICRP soft tissue (ST), ICRP lung tissue (LT), ICRP brain tissue (BT), and ICRU bone (BO) as material

Volume [cm^3]	Absorbed fraction value																			
	0.1 MeV					1 MeV					2 MeV					4 MeV				
	W	ST	LT	BT	BO	W	ST	LT	BT	BO	W	ST	LT	BT	BO	W	ST	LT	BT	BO
0.01	0.958	0.960	0.959	0.960	0.977	0.205	0.215	0.213	0.215	0.401	0.090	0.094	0.094	0.094	0.163	0.043	0.045	0.045	0.045	0.077
0.1	0.981	0.982	0.981	0.982	0.989	0.509	0.526	0.524	0.522	0.701	0.225	0.235	0.234	0.234	0.414	0.101	0.105	0.105	0.104	0.187
1	0.991	0.991	0.991	0.992	0.995	0.755	0.764	0.763	0.761	0.854	0.505	0.520	0.519	0.518	0.692	0.227	0.238	0.236	0.236	0.428
4	0.994	0.995	0.994	0.994	0.997	0.843	0.849	0.849	0.849	0.906	0.669	0.681	0.680	0.680	0.799	0.380	0.395	0.394	0.393	0.605
10	0.996	0.996	0.996	0.996	0.997	0.884	0.888	0.888	0.887	0.931	0.750	0.762	0.759	0.760	0.851	0.506	0.520	0.516	0.518	0.699
20	0.996	0.997	0.996	0.997	0.998	0.907	0.911	0.909	0.909	0.945	0.800	0.806	0.805	0.806	0.879	0.592	0.604	0.605	0.607	0.754
40	0.997	0.997	0.997	0.997	0.999	0.925	0.928	0.928	0.928	0.955	0.839	0.845	0.845	0.844	0.903	0.666	0.680	0.677	0.678	0.801
100	0.998	0.998	0.998	0.998	0.999	0.945	0.947	0.945	0.946	0.996	0.879	0.884	0.882	0.883	0.927	0.748	0.758	0.756	0.756	0.848
500	0.999	0.999	0.999	0.999	0.999	0.967	0.968	0.967	0.968	0.979	0.928	0.930	0.929	0.930	0.955	0.846	0.852	0.850	0.850	0.906
1000	0.999	0.999	0.999	0.999	0.999	0.973	0.974	0.973	0.974	0.983	0.941	0.943	0.943	0.942	0.964	0.875	0.879	0.879	0.880	0.924
6000	0.999	0.999	0.999	0.999	1.000	0.984	0.985	0.985	0.985	0.990	0.966	0.967	0.967	0.967	0.978	0.927	0.930	0.929	0.929	0.955

Table 7. Fitting parameters for a 1 MeV electron for various geometrical models using the logistic model

Model	Parameter								R^2
	A_1		A_2		V_o		P		
Spherical	–0.4673	0.032	0.9925	9.2E-4	0.0140	0.002	0.3910	0.005	0.999
Ellipsoidal	–34.1730	168.920	0.9984	0.001	2.85E-7	4.326E-6	0.3273	0.009	0.999
Cylindrical	–5.5681	4.224	0.9995	5.72E-4	5.89E-5	1.34E-4	0.3194	0.006	0.999

Table 8. Fitting parameters for a 1 MeV γ-photon for various geometrical models employing the Belehradek model fit

Model	Parameter						R^2
	a		B		C		
Spherical	0.0164	1.68E-4	0.0443	0.031	0.3259	0.001	0.999
Ellipsoidal	0.0162	2.284E-4	1	0.238	0.3220	0.002	0.999
Cylindrical	0.0210	0.001	0.8987	0.305	0.2815	0.004	0.997

in good qualitative agreement with earlier findings [15].

The absorbed fraction values have been computed by using Geant4 for various sphere sizes and physics models using different cut values. Table 9 shows that, by changing the cut values, a maximum absolute change of 1.18% in the absorbed fraction value is to be observed. In this study, a range cut of 1 mm appears reasonable for absorbed fraction calculations for various values of target sizes considered here.

CONCLUSIONS

The determination of the absorbed fraction has been carried out using Geant4-based, detailed Monte Carlo simulations. Calculations were carried out for a variety of target geometries, including ellipsoidal, cylindrical, and spherical ones, as well as for a variety of material compositions ranging from soft tissue, water, bone, lung, brain tissue, *etc*. In this work, a comprehensive model has been developed for absorbed frac-

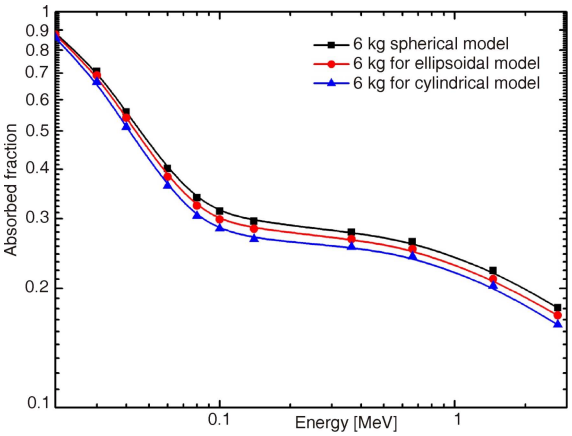

Figure 6. Absorbed fraction for a 6 kg target for uniformly distributed spherical, ellipsoidal, and cylindrical geometrical models using Geant4 simulation

Table 9. Comparison of absorbed fraction values for 20 keV γ-photons in spherical geometry employing the Standard, Penelope, and Livermore Geant4 physics models for indicated secondary cut values

Mass [g]	Standard	Penelope	Livermore
Cut = 1 mm			
0.01	0.0515	0.0540	0.0544
0.1	0.1087	0.1141	0.1140
1	0.2183	0.2299	0.2300
Cut = 0.1 mm			
0.01	0.0514	0.0539	0.0545
0.1	0.1085	0.1141	0.1141
1	0.2179	0.2294	0.2300
Cut = 0.01 mm			
0.01	0.0512	0.0544	0.0538
0.1	0.1079	0.1149	0.1137
1	0.2175	0.2304	0.2293

tion values of various geometries, incorporating both electrons and gamma rays:

– the values of absorbed fractions show a decreasing trend moving away from spherical – to ellipsoidal – to cylindrical geometries, while the target size remains fixed,
– gamma-ray absorbed fraction values have been found to be sensitive to the material composition of the targets, especially at low energies, while for elections, the absorbed fraction values remain insensitive to low energy values, and
– the variation of absorbed fraction values in relation to target volumes has been found to follow logistic behavior for electrons and Belehradek's equation for gamma-rays.

AUTHOR CONTRIBUTIONS

Theoretical analysis was carried ou by Z. Rahman, S. U. Rehman, and W. Arshed, and modeling and comparisons were done by Z. Rahman, S. M. Mirza, and N. M. Mirza. All authors contributed towards analysis and discussion. The manuscript written Z. Rahman, S. M. Mirza, N. M. Mirza, and W. Arshed. The figures were prepared by Z. Rahman and S. U. Rehman.

REFERENCES

[1] Allison, J., *et al*., Geant4 Development and Applications, *IEEE Transactions on Nuclear Science, 53* (2006), 1, pp. 270-278
[2] Johnson, T. K., MABDOSE: A Generalized Program for Internal Radionuclide Dosimetry, *Comp. Methods Programs Biomed., 27* (1988), 2, pp. 159-167
[3] ***, ICRP, Limits for Intakes of Radionuclides by Workers, ICRP Publication 30, part 1, Pergamon Press, Oxford, UK, 1979
[4] Bolch, W. E, *et al*., MIRD Pamphlet 21: A Generalized Schema for Radiopharmaceutical Dosimetry-Standardization of Nomenclature, *Journal of Nuclear Medicine, 50* (2009), 3, pp. 477-484
[5] Loevinger, R., Berman, A. A., A Revised Schema for Calculating the Absorbed Dose from Biologically Distributed Radionuclides, MIRD Pamphlet No. 1, Society of Nuclear Medicine, New York, USA, 1976
[6] Ford, R. L., Nelson, W. R., The EGS Code System -Version 3, Stanford Linear Accelerator Center Report SLAC-210, 1978
[7] Briesmeister, J. F., MCNP-A General Monte Carlo N-Particle Transport Code, Version 4B, Los Alamos National Laboratory Report No. LA-12625-M, 1997
[8] Berger, M. J., Distribution of Absorbed Dose Around Point Sources of Electrons and Beta Particles in Water and Other Media, *Journal of Nuclear Medicine, 12* (1971), 5, pp. 5-23
[9] Brownell, G. L., Ellen, W. H., Reddy, A. R., The Society of Nuclear Medicine: MIRD Pamphlet 3. *Journal of Nuclear Medicine, 9* (1968), Suppl. 1, pp. 27-39
[10] Akabani, G., Poston, J. W., Bolch, W. E., Estimates of Beta Absorbed Fractions in Small Tissue Volumes for Selected Radionuclides, *Journal of Nuclear Medicine, 32* (1991), 5, pp. 835-839
[11] Stabin, M. G., Konijinenberg, M. W., Re-Evaluation of Absorbed Fractions for Photons and Electrons in Spheres of Various Sizes, *Journal of Nuclear Medicine, 41* (2000), 1, pp. 149-160
[12] Agostinelli, S., *et al*., Geant4-a Simulation Toolkit, Nuclear Instruments and Methods in Physics Research Section A: Accelerators, Spectrometers, *Detectors and Associated Equipment, 506* (2003), 3, pp. 250-303
[13] Amato, E., Lizio, D., Baldar, S., Absorbed Fractions for Electrons in Ellipsoidal Volumes, *Physics in Medicine and Biology, 56* (2011), 2, pp. 357-365
[14] Amato, E., Lizio, D., Baldar, S., Absorbed Fractions for Photons in Ellipsoidal Volumes, *Physics in Medicine and Biology, 54* (2009), 20, pp. N479-N487
[15] Yoriyaz, H., *et al*., Physical Models, Cross-Sections, and Numerical Approximations Used in MCNP and Geant4 Monte Carlo Codes for Photon and Electron Absorbed Fraction Calculation, *Medical Physics, 36* (2009), 11, pp. 5198-5213
[16] Barca, G., *et al*., A Powerful Simulation Tool for Medical Physics Applications: Geant4, *Nuclear Physics B (Proc. Suppl.), 125* (2003), pp. 80-84
[17] ***, ICRU37, Stopping Powers for Electrons and Positrons (Icru Report 37; International Commission on Radiation Units and Measurements), *Nuclear In-*

struments and Methods in Physics Research Section B, 12 (1985), 1, pp. 187-188
[18] Berger, M. J, H. J. H., Seltzer, S. M, XCOM: Photon Cross-Sections Database, NIST Standard Reference Database 8 (XGAM), 2011
[19] Cirrone, G. A. P., *et al*., Validation of the Geant4 Electromagnetic Photon Cross-Sections for Elements and Compounds, *Nuclear Intruments and Methods in Physics Research, Section-A, 618* (2010), 1-3, pp. 315-322
[20] McLAREN, I. A., Predicting Development Rate of Copepod Eggs, *The Biological Bulletin, 131* (I966), 3, pp. 457-469
[21] ***, ICRP, Radiation Dose to Patients from Radiopharmaceuticals, in ICRP Publication 53, Pergamon Press, Oxford, UK, 1988

Received on February 11, 2013
Accepted on December 11, 2013

**Зиаур РАХМАН, Шакил Ур РЕХМАН, Сикандер М. МИРЗА,
Вахид АРШЕД, Насир М. МИРЗА**

ЦЕЛОВИТА СТУДИЈА АПСОРБОВАНЕ КОЛИЧИНЕ ЕЛЕКТРОНА И ГАМА ФОТОНА ЗАСНОВАНА НА Geant4 ПРОГРАМУ КОРИШЋЕЊЕМ РАЗЛИЧИТИХ ГЕОМЕТРИЈСКИХ МОДЕЛА И БИОЛОШКИХ ТКИВА

Развијен је модел заснован на Geant4 програму за предвиђање вредности апсорбоване количине електрона и гама фотона у сферној, елипсоидној и цилиндричној геометрији. Симулација је изведена за воду, меко, мождано, плућно и коштано ICRP ткиво, за електроне енергија од 0.1 MeV до 4 MeV и гама фотоне из опсега енергија од 0.02 MeV до 2.75 MeV. Сагласно са експерименталним закључцима, симулиране вредности опадају са порастом енергије зрачења. У поређењу са NIST XCOM и ICRU подацима, симулиране вредности помоћу Geant4 програма не одступају више од 4.2% односно 1.6%, респективно. За електроне и гама фотоне, релативно одступање предвиђања заснованих на Geant4 моделу у односу на референтну реевалуацију не прелази 6.8% и 7.4%, респективно. Елипсоидни и цилиндрични модели показују веће вредности дела апсорбоване дозе у односу на сферични модел. Примећено је да зависност циљане запремине од вредности апсорбованог дела прати очекивано понашање електрона и Белерадекову једначину за гама фотоне. Вредности апсорбоване количине гама фотона осетљиве су на материјал од којег је мета направљена, нарочито на ниским енергијама, за разлику од електрона код којих ово понашање није уочено.

Кључне речи: Geant4 симулација, депонована енергија, унутрашња дозиметрија, апсорбована фракција